High-pressure phases, vibrational properties, and electronic structure of $Ne(He)_2$ and $Ar(He)_2$: A first-principles study

C. Cazorla,[1,2] D. Errandonea,[3] and E. Sola[2]
[1]*Materials Simulation Laboratory, UCL, London WC1H OAH, United Kingdom*
[2]*Department of Earth Sciences, UCL, London WC1E 6BT, United Kingdom*
[3]*Departamento de Física Aplicada, ICMUV–Fundacio General Universitat de Valencia, 46100 Burjassot (Valencia), Spain*
(Received 29 April 2009; revised manuscript received 30 June 2009; published 10 August 2009)

We have carried out a comprehensive first-principles study of the energetic, structural, and electronic properties of solid rare-gas (RG)-helium binary compounds, in particular, $Ne(He)_2$ and $Ar(He)_2$, under pressure and at temperatures within the range of $0 \leq T \leq 2000$ K. Our approach is based on density-functional theory and the generalized gradient approximation for the exchange-correlation energy; we rely on total Helmholtz free-energy calculations performed within the quasiharmonic approximation for most of our analysis. In $Ne(He)_2$, we find that at pressures of around 20 GPa the system stabilizes in the $MgZn_2$ Laves structure, in accordance to what was suggested in previous experimental investigations. In the same compound, we predict a solid-solid phase transition among structures of the Laves family of the type $MgZn_2 \rightarrow MgCu_2$, at a pressure of $P_t = 120(1)$ GPa. In $Ar(He)_2$, we find that the system stabilizes in the $MgCu_2$ Laves phase at low pressures but it transitates toward the AlB_2-type structure by effect of compression at $P_t = 13.8(4)$ GPa. The phonon spectra of the $Ne(He)_2$ crystal in the $MgZn_2$ and $MgCu_2$ Laves structures, and that of $Ar(He)_2$ in the AlB_2-type phase, are reported. We observe that the compressibility of RG-RG and He-He bond distances in $RG(He)_2$ crystals is practically identical to that found in respective RG and He pure solids. This behavior emulates that of a system of noninteracting hard spheres in closed-packed configuration and comes to show the relevance of short-range interactions on this type of mixtures. Based on size-ratio arguments and empirical observations, we construct a generalized phase diagram for all $RG(He)_2$ crystals up to a pressure of 200 GPa where we map out systematic structural trends. Excellent qualitative agreement between such generalized phase diagram and accurate *ab initio* calculations is proved. A similar construction is done for $RG(H_2)_2$ crystals; we find that the $MgCu_2$ Laves structure, which has been ignored in all RG-H_2 works so far, might turn out to be competitive with respect to the $MgZn_2$ and AlB_2-type structures. Furthermore, we explore the pressure evolution of the energy-band gap in $RG(He)_2$ solids and elaborate an argument based on electronic-band theory which explains the observed trends.

DOI: 10.1103/PhysRevB.80.064105 PACS number(s): 61.50.Ah, 64.70.K−, 64.75.Ef, 65.40.−b

I. INTRODUCTION

Understanding the behavior of rare gases (RGs) and their mixtures under pressure is of relevance in astronomy and planetary sciences because of their abundance in universe and presence in the interior of planets and stars. Additionally, rare-gas solids are also of interest for practical applications. Light RGs are inert solids with intriguing elastic properties and very small bulk modulus[1,2] so alloys involving them may lead to new class of materials of potential use in science and technology (for instance, as improved pressure-transmitting media in high-load compression experiments and/or synthesis processes). Therefore, information about the structural, electronic, and vibrational properties of systems such as binary mixtures of RGs and He is desirable. Among the binary mixtures of RGs and He, only the Ne-He system has been studied.[3,4] Indeed, there is experimental evidence for the stabilization of a homogeneous Ne-He binary crystal at moderate pressures (10 GPa $< P$), with a ^{4}He molar concentration of 2/3. From synchrotron x-ray diffraction measurements, the phase structure of such compound was identified, though not unequivocally, with the $MgZn_2$ Laves structure (C14).[3] Nevertheless, a satisfactory exploration of the phase diagram of $Ne(He)_2$ and of RG-He compounds in general is still lacking and structural solid-solid phase transitions are expected to appear on them by effect of pressure.

From the crystallographic point of view, mixtures of RGs and He are interesting systems because they appear to crystallize in a series of structures belonging to a particular class of alloys, the so-called Laves phases.[5–8] These structures have composition AX_2 and are considered as size-factor compounds, forming the largest group of intermetallic alloys with more than 1400 representatives. An important characteristic of the Laves phases is that the thermodynamic $P-V$ ranges over which they become stable may be understood in terms of space-filling arguments. This implies that changing atom A in compound AX_2 by an element with larger or smaller atomic radius may induce a solid-solid phase transition between structures belonging to the Laves family. In the same way, thermodynamic pressure may act as the driving force of such structural changes. Pressure effects on the crystalline structure of compounds such as $Ne(He)_2$ and $Ar(He)_2$, therefore, are interesting not only for basic research but for understanding the nature of many Laves-type intermetallic compounds which show remarkable mechanical and physical properties.

Concerning the electronic properties, RGs are known to be good insulators at normal conditions of temperature and pressure though they are expected to become eventually semiconductor or even metallic by effect of extreme compression.[9] The case of RG-He compounds is particularly interesting because possible pressure-induced metallization

of helium due to chemical precompression by heavier elements. In addition to this, one can do reasonable extrapolations to the electronic and structural properties of RG-$(H_2)_2$ systems, much more intensively studied so far,[10–14] basing on RG-$(He)_2$ results.

It is worthwhile noticing that from a theoretical point of view light RG crystals are challenging systems to describe since, despite their electronic structure is simple, one has to deal with related anharmonicity and zero-point motion even in the regime of low temperatures.[15,16] Moreover, long-range correlations of van der Waals type play a decisive role in their cohesion at low densities and standard first-principles techniques such as density-functional theory (DFT) may fail at reproducing such type of interactions.[17–19] For these reasons, RG solids are challenging and special benchmarks for first-principles work.

In this work, we present a comprehensive first-principles study of the structural, vibrational, and electronic properties of solid $Ne(He)_2$ and $Ar(He)_2$ binary compounds under pressure. We also provide information about the energetic and electronic properties of the $Kr(He)_2$ crystal but to a lesser extent. To the best of our knowledge, previous studies characterizing solid $Ar(He)_2$ and $Kr(He)_2$ are inexistent so this work provides among other things motivation to further experimental and theoretical research. Our computational approach is based on DFT and we have performed zero temperature and quasiharmonic Helmholtz free-energy calculations over wide thermodynamic ranges (typically, $0 \leq P \leq 300$ GPa and $0 \leq T \leq 2000$ K). As a result, here we report on the prediction of phase transitions and we map out systematic structural trends in the high-P phase diagram of RG-He mixtures. Furthermore, results for the vibrational phonon spectra and the evolution of the electronic-band gap with pressure in $Ne(He)_2$ and $Ar(He)_2$ are presented.

The remainder of the paper is organized as follows. In the next section, we provide a brief description of the Laves and AlB_2-type structures since these are nonstandard crystal phases to which the reader may be not familiarized and are relevant to RG-He systems. In Sec. III, the basics of the computational methods used and technicalities are summarized. Then (Sec. IV), we move to present our zero- and finite-temperature results for the $Ne(He)_2$ and $Ar(He)_2$ crystals and general structural and electronic trends found in RG-He mixtures under pressure. A discussion about $RG(H_2)_2$ crystals based on $RG(He)_2$ results is reported in Sec. V together with the conclusions.

II. CRYSTAL STRUCTURES

Many AX_2 compounds involving large A atoms and small X atoms crystallize in the Laves phases or in the AlB_2-type structure.[5–8] These structures have been considered in the literature as the potential structures for $RG(He)_2$ compounds[3] and will be the ones considered along this work. All these phases involve a maximization of packing fraction. When the atomic diameters d_A and d_X have a ratio slightly smaller than $\sqrt{3/2}$, AX_2 alloys usually crystallizes in the hexagonal C14 Laves structure, typified by $MgZn_2$ (space group: $P63/mmc$, $Z=4$). In the case that d_A/d_X is slightly larger than $\sqrt{3/2}$,

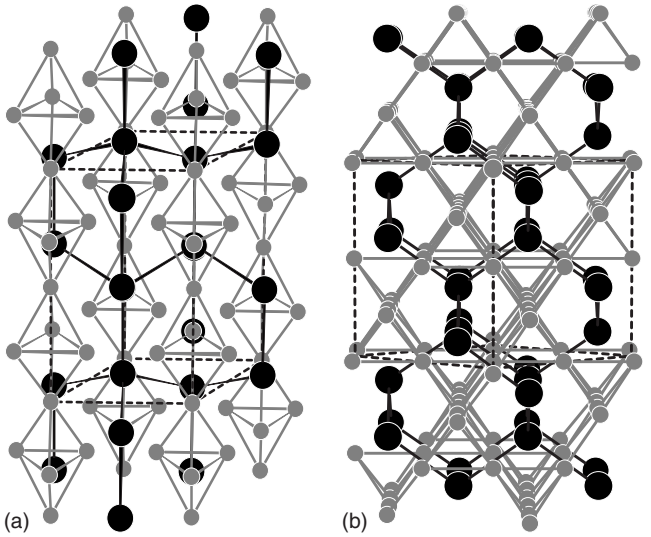

FIG. 1. Schematic representation of the $MgZn_2$ (a) and $MgCu_2$ (b) crystal structures. Large black spheres represent RG atoms while small gray spheres represent ^{4}He atoms.

then the cubic C15 Laves structure (space group: $Fd3m$, $Z=8$), typified by $MgCu_2$, is favored. On the other hand, when the value of this ratio is between 1.4 and 1.6 the elements mixtures prefer the hexagonal AlB_2-type structure (space group: $P63/mmc$, $Z=1$). In addition to these structures, the hexagonal C36 Laves phase is also commonly found, typified by $MgNi_2$ (space group: $P63/mmc$, $Z=8$). The Laves phases, shown in Figs. 1 and 2, can be described in terms of hexagonal lattices in which atomic arrangements lead to the assumption of axial ratios in proportion 2:3:4 for $MgZn_2$,

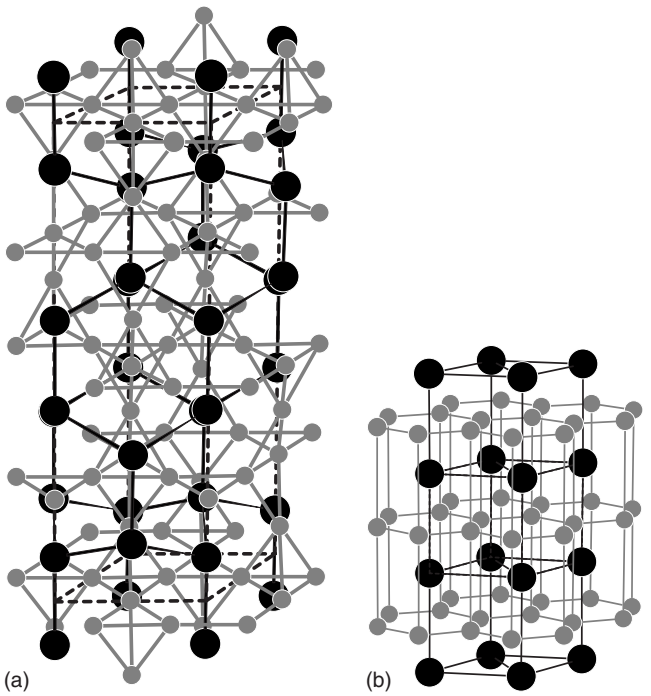

FIG. 2. Schematic representation of the $MgNi_2$ (a) and AlB_2-type (b) crystal structures. Large black spheres represent RG atoms while small gray spheres represent ^{4}He atoms.

$MgCu_2$, and $MgNi_2$, respectively. They can be regarded also as tetrahedrally close-packed structures of atoms *A* and *X*. Large *A* atoms are surrounded by 16 vertices Frank-Kasper polyhedron (12 *X* and 4 *A* atoms) and small *X* atoms are surrounded by an icosahedron formed by 6 *A* atoms and 6 *X* atoms. In each case, the main difference is the ordering of the *X* atoms tetrahedra. In the $MgZn_2$ structure, they join alternatively point-to-point and base-to-base (see top of Fig. 1). In the $MgCu_2$ structure, they join point-to-point (see bottom of Fig. 1) and structure $MgNi_2$ contains both types of junctions (see top of Fig. 2). In the three phases the *A* atoms are accommodated within the holes of the arrangement of tetrahedra, forming a hexagonal network. Regarding the AlB_2-type structure,[20] this can be understood as a distorted version of the $MgCu_2$ phase. This structure is shown in Fig. 2 (bottom) where a close-packed arrangement of *A* and *X* atoms can be seen. Basically, it consists of a graphitelike layered *X* atom structure between which *A* atoms accommodate forming intermediate triangular lattices.

III. METHODS AND TECHNICALITIES

DFT is a first-principles approach which has allowed for accurate and reliable knowledge of a great deal of materials with exceptional computational affordability.[21,22] In this work, DFT provides the basis for our understanding of the atomic and electronic structure of RG-He crystals as a function of pressure. There is only one uncontrollable approximation in DFT, namely, the functional used for the exchange-correlation energy E_{xc}. There is abundant evidence that commonly used E_{xc} functionals yield accurate results for a range of properties of metallic and nonmetallic crystals, including equilibrium lattice parameter, elastic constants, phonon frequencies, $T=0$ equation of state (EOS), solid-state phase boundaries, etc.[15,23,24] The exchange-correlation functional used for all the present work is that due to Perdew and Wang,[25] which provides very good agreement with respect to experimental $P-V$ data found in Ref. 3 [better than obtained with the local-density approximation (LDA) due to Ceperley and Alder,[26] as we have checked].

A completely separate issue from the choice of E_{xc} is the implementation of DFT that is used. This concerns mainly the way that the electron orbitals are represented. There are several implementations of DFT that can be used to calculate the total energy per atom of a crystal, including pseudopotential techniques,[27] the projector augmented wave (PAW) technique,[28,29] the full-potential augmented plane-wave technique,[30,31] etc. We have chosen to use PAW here, as implemented in the VASP code[32] because it has been shown that for a given E_{xc} functional it can give values for the total energy that are closer to the exact value than most other implementations.[33]

We calculate the total Helmholtz free energy $F_{tot}(V,T)$ of RG-He crystals within the quasiharmonic approximation using the formula

$$F_{tot}(V,T) = E_{perf}(V,0) + F_{harm}(V,T), \quad (1)$$

where E_{perf} is the energy of the perfect (relaxed) static crystal at zero temperature and F_{harm} is the part of the total energy which stems from the atomic vibrational excitations and, that is, calculated using the phonon frequencies. In this section, we briefly explain the basics of the methods that we have used for estimating F_{tot} and summarize the parameters and settings that control convergence in our results.

Before moving to this, it must be noted that standard DFT may give poor results at describing long-range dispersive interactions, such as for instance van der Waals forces, due to the local nature of the approximations introduced.[17–19] Also, it is well known that such interactions play an important role in the cohesion of RG solids at low densities. Nevertheless, short-range effects in RG systems become increasingly more relevant as pressure is raised so the description obtained with DFT becomes progressively more accurate as density is increased.[34] In fact, Nabi *et al.*[35] have shown recently that the elastic properties and equation of state of solid ^{4}He calculated with DFT are in very good agreement with respect to measurements performed at $P \geq 13$ GPa. For these reasons, and despite dispersive interactions have not been treated in any specific way, the results we are to present here should be considered as accurate since we have restricted our analysis to the regime of intermediate and high pressures (which we somehow arbitrarily set as $P \geq 12$ GPa). Questions such as, which is the minimum pressure at which solid $Ne(He)_2$ and $Ar(He)_2$ stabilize? and what are the stable structures of these crystals at low pressures ($P \leq 12$ GPa)? cannot be answered satisfactorily with the present approach, so we leave them for future work.

A. Zero-temperature energy calculations

There is a series of parameters that control convergence in our PAW calculations. Essentially, these are the number of *k* points used for integration over the first Brillouin zone (BZ), maximum energy cutoff for the plane-wave basis set, number and type of electrons considered in valence, smearing of the Fermi-Dirac electronic occupation distribution, and the tolerance for energy convergence in the self-consistency cycle. Based on exhaustive tests, we have set the value of all these parameters so as to ensure convergence of the total electronic energy E_{perf} to less than 0.1 meV/atom.[36] As will be shown in the next section, energy differences among the Laves structures turn out to be very small [especially in the case of $Ne(He)_2$] so we have chosen large energy cutoffs and dense *k*-point grids. In particular, we use special Monkhorst-Pack (MP) *k*-point grids[37] of $14\times14\times7$ for the $MgZn_2$ structure (12 atoms per unit cell), $14\times14\times14$ for the $MgCu_2$ structure (6 atoms per unit cell), $12\times12\times4$ for the $MgNi_2$ structure (24 atoms per unit cell) and $9\times9\times18$ for the AlB_2-type structure (3 atoms per unit cell). The plane-wave energy cutoff chosen for the different elements is, 480.0 eV for $He(1s^2)$, 412.4 eV for $Ne(2s^22p^6)$, 319.6 eV for $Ar(3s^23p^6)$, and 222.4 eV for $Kr(4s^24p^6)$, where the number within parentheses indicate the electronic states considered in valence. A tolerance of 10^{-5} eV for the self-consistent loops and Fermi-Dirac smearing equivalent to an electronic temperature of 2000 K, has been imposed.

For a given volume of the unit cell, the equilibrium position of the atoms in the $MgZn_2$-, $MgNi_2$-, and AlB_2-type

structures are not entirely determined and ionic relaxation loops must be carried out in order to minimize the forces acting on each atom. We have done this by using a conjugate-gradient algorithm which allows for atomic and cell shape variation while keeping the volume fixed, and we have imposed a tolerance in the atomic forces of 0.01 eV/Å. Several tests have been carried out on this setting and the conclusion emerging from them is that by imposing atomic forces tolerances down to 0.005 eV/Å our results remain unaltered.

The total electronic zero-temperature energy $E_{\rm perf}$ [see Eq. (1)] of $Ne(He)_2$ and $Ar(He)_2$ in the $MgZn_2$-, $MgCu_2$-, $MgNi_2$-, and AlB_2-type crystal structures, has been calculated over grids of typically 12 volume-points distributed uniformly within the pressure range of $0 \leq P \leq 300$ GPa. Atomic cell relaxations have been performed for all the structures at every single volume point (except for the $MgCu_2$ structure). Energy results then have been fitted to a third-order Birch-Murnaghan equation,[38] which reads

$$E_{\rm perf}(V,0) = E_0 + \frac{3}{2}V_0K_0\left[-\frac{\chi}{2}\left(\frac{V_0}{V}\right)^2 + \frac{3}{4}(1+2\chi)\left(\frac{V_0}{V}\right)^{(4/3)} - \frac{3}{2}(1+\chi)\left(\frac{V_0}{V}\right)^{(2/3)} + \frac{1}{2}\left(\chi+\frac{3}{2}\right)\right], \quad (2)$$

where E_0 and $K_0 = -V_0\frac{d^2E}{dV^2}$ are the values of the energy and the bulk modulus at equilibrium volume V_0, respectively, $\chi = \frac{3}{4}(4-K_0')$ and $K_0' = [\partial K/\partial P]$, with derivatives evaluated at zero pressure. The static ($T=0$) equation of state is obtained as the minus derivative of Eq. (2) as a function of volume. A zero-temperature phase transition between stable crystal structure *I* and energetically competitive crystal structure *II* will occur at pressure P_t, when the corresponding enthalpies of both phases become equal [that is, $P_I(V_I) = P_{II}(V_{II}) = P_t$ and $E_{\rm perf}(V_I) + P_tV_I = E_{\rm perf}(V_{II}) + P_tV_{II}$].

B. Atomic vibrational energy

We have calculated the phonon-dispersion relations of $Ne(He)_2$ in the $MgZn_2$ and $MgCu_2$ structures and of $Ar(He)_2$ in the AlB_2-type structure (for reasons that will become clear later) at a series of volumes. In particular, we have considered a volume range of $2.90 \leq V \leq 9.01$ Å^3 (6 volume-point grid) for $Ne(He)_2$ and $4.43 \leq V \leq 9.53$ Å^3 (4 volume-point grid) for $Ar(He)_2$. These have been calculated using the PHON code[39,40] which implements the small displacement method described in Refs. 41 and 42. With this method, the quantity which is directly calculated is the force-constant matrix $\Phi_{i\alpha,j\beta}(\mathbf{R_{ij}})$, where $\mathbf{R_{ij}}$ is the position vector connecting atoms labeled i and j in the crystal and α,β indicate Cartesian coordinates. This can be evaluated by displacing selected atoms in one primitive cell by a small amount and computing the forces induced on all the other atoms in the system. The force-constant matrix is then the constant of proportionality between the displacement and the forces. Atomic forces are calculated with the VASP code[32] and within the PAW scheme.[28,29] The phonon frequencies $\omega_{\mathbf{q}s}$ for any $\mathbf{q}$ vector in the BZ and branch s, are obtained as eigenvalues of the dynamical matrix which is given by

$$D_{i\alpha,j\beta}(\mathbf{q}) = \frac{1}{\sqrt{m_im_j}}\sum_{\mathbf{R_{ij}}}\Phi_{i\alpha,j\beta}(\mathbf{R_{ij}})\exp[i\mathbf{q}\cdot\mathbf{R_{ij}}], \quad (3)$$

where m_i is the mass of the ith atom and the sum has to be evaluated for every lattice vector $\mathbf{R_{ij}}$ in the crystal. In fact, $\Phi(\mathbf{R})$ is usually short ranged and therefore one only needs to include in the sum those terms for which $\Phi(\mathbf{R})$ is appreciably different from zero. This makes the small displacement method feasible, as one only needs $\Phi(\mathbf{R})$ in a finite supercell. Convergence of the phonon frequencies $\omega_{\mathbf{q}s}$ is then ensured by progressively increasing the size of the supercell used to evaluate $\Phi(\mathbf{R})$.

In metallic and semimetallic systems, the force-constant matrix, and therefore the phonon frequencies, may depend on temperature because of electronic excitations. In this work, however, we neglect such dependence because we are dealing with nonmetallic crystals and the temperature range considered is in any case not too wide ($0 \leq T \leq 2000$ K).

We have tested the convergence of the phonon frequencies with respect to a number of technical parameters. The quantity used to measure the quality of the results is the ionic free-energy in the quasiharmonic approximation, given by

$$F_{\rm harm}(V,T) = \frac{1}{N_{\mathbf{q}}}k_BT\sum_{\mathbf{q},s}\ln\left\{2\sinh\left[\frac{\hbar\omega_{\mathbf{q}s}(V,T)}{2k_BT}\right]\right\}, \quad (4)$$

where the sums are over phonon wave vectors $\mathbf{q}$ in the BZ and branches s, and $N_{\mathbf{q}}$ is the number of $\mathbf{q}$ points in the sum. First, we tested the size of the displacement, which has to be small in order to be in the validity range of the harmonic approximation but also big enough so that the forces induced in the crystal are not too small compared to the numerical noise in the calculations. We found that a value of 0.04 Å is a good compromise and allows us to obtain free energies at 300 K converged within 1 meV/atom. The calculations were done using a single $MgCu_2$ unit cell (six atoms). Second, we tested convergence with respect to k-point sampling, and we found that a $12\times12\times12$ MP k-point grid is necessary to obtain free energies converged within 1 meV/atom at 300 K. Third, we tested the size of the supercell and found that the convergence of the vibrational free energy was obtained using cells containing at least 162 atoms ($3\times3\times3$) for the $MgCu_2$ structure. Finally we did convergence tests on the grid of $\mathbf{q}$ points in which the phonons are calculated and found that a $20\times20\times20$ $\mathbf{q}$-point grid is necessary for having a convergence under 1 meV/atom in the quasiharmonic free energy.

The Laves phases are low-symmetry structures with a large number of atoms in the unit cell so calculation of the corresponding phonon frequencies is a quite demanding computational task. For this reason, we have not repeated convergence tests in the rest of structures but adapted somehow the settings already obtained for the $MgCu_2$ structure to them. In particular, we have used $2\times2\times2$ supercell (96 atoms) and $6\times6\times4$ MP k-point grid for the $MgZn_2$ structure, and $4\times4\times3$ (144 atoms) and $4\times4\times4$, respectively, for the AlB_2-type structure.

The finite-temperature $P-V$ curves we are to report have been obtained as the minus derivative of $F_{\rm tot}(V,T)$ with re-

spect to volume. At given temperature T and pressure P_t, a phase transition between stable *(I)* and competitive *(II)* crystal structures occurs whether the Gibbs free energy of both phases are equal [that is, $P_I(V_I)=P_{II}(V_{II})=P_t$ and $F_{\text{tot}}(V_I)+P_tV_I=F_{\text{tot}}(V_{II})+P_tV_{II}$]; this is the condition that we have imposed in order to obtain the finite-temperature solid-solid phase transitions that we report in Sec. IV.

IV. RESULTS

In this section, we present first results and analysis of the energetic and structural properties of solid $Ne(He)_2$ and $Ar(He)_2$. Then, we use the results and conclusions obtained to propose a general and qualitative zero-temperature phase diagram of all $RG(He)_2$ binary compounds under pressure. Next, we analyze the electronic structure and evolution of the electronic-band gap as a function of pressure in $Ne(He)_2$, $Ar(He)_2$, and $Kr(He)_2$, and present an argument based on electronic-band theory to explain the trends that are observed.

A. $Ne(He)_2$

In Fig. 3 (top), we enclose zero-temperature enthalpy energy differences, ΔH, of the $Ne(He)_2$ crystal in the $MgZn_2$ structure with respect to the $MgCu_2$ and $MgNi_2$ Laves phases, as a function of pressure. For a given pressure P, $Ne(He)_2$ will stabilize in the $MgZn_2$ structure if $\Delta H(P)\leq 0$, or contrarily, in the Laves structure of largest $\Delta H(P)$. The AlB_2-type structure has been considered up to a pressure of $\sim$1150 GPa but found to be energetically not competitive ($\Delta H\leq -0.05$ eV/atom), so for the sake of clarity we disregard this crystal structure in our subsequent analysis. As one can see in Fig. 3 (top), enthalpy energy differences among the Laves structures turn out to be very small however our stringent accuracy threshold of 0.1 meV/atom in the calculation of the energies ensures the reliability of these results. Reassuringly, ΔH curves obtained both with LDA (not shown here) and GGA approximations are well behaved and show monotonic trends. Uncertainties associated to the estimation of the equation of state are calculated by performing error propagation analysis over the expression enclosed in Eq. (2).

It is shown that at $T=0$ and up to a pressure of $P_t=120(1)$ GPa (where 1 GPa is the error associated to our estimation of P_t) solid $Ne(He)_2$ remains stable in the $MgZn_2$ structure while $MgCu_2$ is energetically the most competitive crystal phase. This result confirms the suggestion made by Loubeyre *et al.*,[3] who found evidence for the stabilization of $Ne(He)_2$ at pressures of 13.7 and 21.8 GPa and performed synchrotron x-ray diffraction measurements and semiempirical calculations in order to resolve its corresponding atomic structure. Figure 3 (bottom) also shows $P-V$ isotherms calculated at zero-temperature and $T=296$ K. As is observed, the agreement between experiments (performed at $T=296$ K) and our results is fairly notable though our calculations systematically overestimate pressure by a small amount (in particular, 1.9 GPa at $V=7.89$ Å^3 and 4.2 GPa at $V=6.89$ Å^3). The value of the parameters that result from

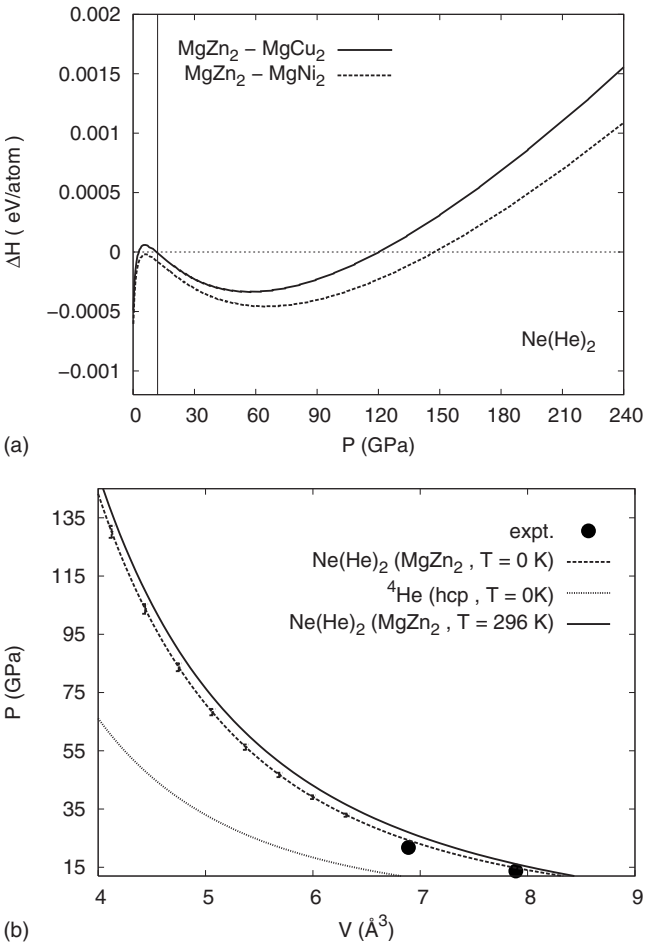

FIG. 3. Top: enthalpy energy difference, ΔH, between the $MgZn_2$, $MgCu_2$, and $MgNi_2$ Laves phases of $Ne(He)_2$ at zero temperature and as a function of pressure. The vertical solid line at 12 GPa separates the low pressure from the intermediate and high-pressure regimes. Uncertainties associated to ΔH amount to 0.1 meV/atom. Bottom: equation of state of $Ne(He)_2$ in the $MgZn_2$ phase structure calculated at $T=0$ and 296 K (uncertainties associated to the zero-temperature case are represented with vertical dashed lines). Experimental data and previous zero-temperature calculations of solid ^{4}He in the hcp crystal phase are shown for comparison.

fitting the polynomial function expressed in Eq. (2) to our zero-temperature results is $E_0=-0.0313(0.0009)$ eV, $V_0=18.35(0.20)$ Å^3, $K_0=0.0134(0.0007)$ eV/Å^3 [=2.15(0.11), in GPa], and $\chi=-0.578(0.019)$, where figures within parentheses indicate the associated error. In the same figure, the zero-temperature EOS of bulk solid ^{4}He found in Ref. 15 is shown for comparison; as can be seen from the slope of the $P-V$ curves, the $Ne(He)_2$ crystal is less compressible than bulk solid ^{4}He (that is, the quantity $\frac{1}{V}\frac{\partial V}{\partial P}$ is larger in helium) and this difference appears to increase with raising pressure. Despite of this, the calculated bulk modulus of $Ne(He)_2$, $K_0=2.15(0.11)$ GPa, turns out to be smaller than that of many other materials which are standardly used as pressure-transmitting media in high-load compression experiments[43,44] and synthesis processes [as for instance, argon, with $K_0=6.50$ GPa,[45] and neon, with $K_0=2.75$ GPa

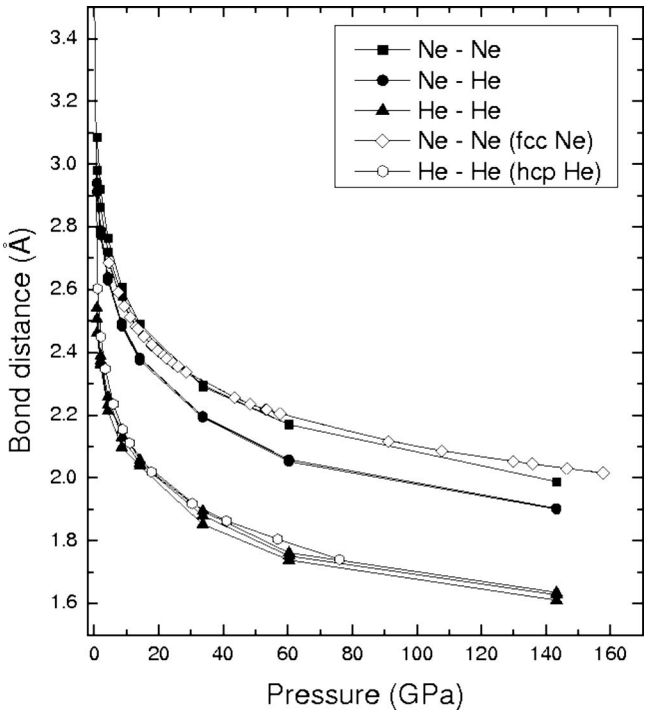

FIG. 4. Pressure-induced variation of atomic He-He, He-Ne, and Ne-Ne bond distances in the $Ne(He)_2$ crystal ($MgZn_2$ structure). Evolution of atomic bond distances in pure ^4He and Ne bulk systems are shown for comparison.

(Ref. 34)]. Therefore, binary mixtures of Ne and He appear to be very well-suited materials for ensuring hydrostatic conditions in high-pressure research.

It is also interesting to note the differential compressibility of the He-He and Ne-Ne bonds. In particular (see Fig. 4), we show that the He-He bonds are the most compressible and that for a given pressure P the equilibrium He-He and Ne-Ne pairwise distances are practically identical to those found in pure solid He and solid Ne, respectively. This result comes to show that $Ne(He)_2$ apparently behaves as two independent interpenetrating atomic substructures which *do not interact among themselves*. This same behavior is also observed in solid $Ar(He)_2$. We will comment again on this finding in Sec. IV C.

In Table I, we report the value of the $4f$ (z_2, occupied by a Ne atom) and $6h$ (x_1, occupied by a He atom) Wyckoff positions and c/a ratio in the $MgZn_2$ structure as a function of pressure. As can be seen, positions z_2 and x_1 do not vary significantly with pressure whereas the value of the c/a ratio increases steadily and saturates to 1.633 at high pressures. These atomic rearrangements have the overall effect of making the $MgZn_2$ structure more symmetric. This is shown in Fig. 4, where we have plot He-He, He-Ne, and Ne-Ne interatomic pairwise distances of the $Ne(He)_2$ crystal in the $MgZn_2$ structure as a function of pressure: beyond a pressure of ~35 GPa the two first Ne-Ne nearest-neighbor distances (also the He-He and Ne-He ones) become increasingly more similar, which is a clear signature for the increase in symmetry.

TABLE I. Pressure evolution of the $4f$ and $6h$ Wyckoff positions (z_2 and x_1, respectively) and c/a ratio of $Ne(He)_2$ in the $MgZn_2$ crystal structure.

P(GPa)	z_2	x_1	c/a
142.30	0.062549	0.832061	1.6336
68.30	0.062641	0.831733	1.6333
33.77	0.062780	0.831469	1.6312
14.21	0.063443	0.831174	1.6301
8.61	0.064341	0.830338	1.6264
4.30	0.062438	0.830602	1.6282

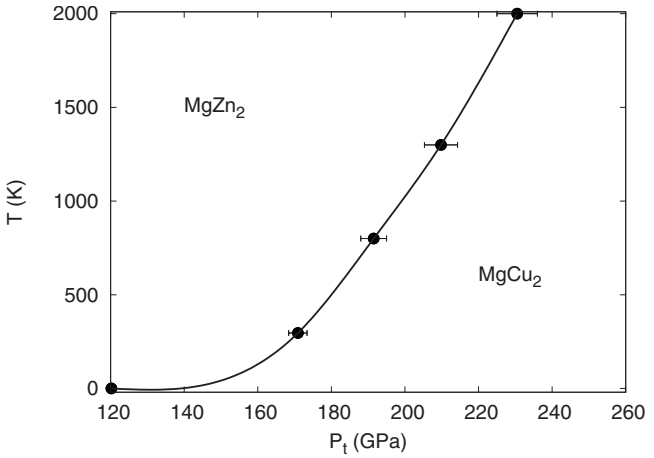

FIG. 5. Calculated $MgZn_2 \rightarrow MgCu_2$ phase boundary in $Ne(He)_2$ as a function of temperature. The solid line is a guide for the eye which connects the points of the solid-solid phase boundary explicitly calculated (solid circles). Uncertainties associated to our calculations are shown in the plot with horizontal solid lines.

Coming back to Fig. 3, there is shown that at a pressure of $P_t = 120(1)$ GPa and zero temperature the $Ne(He)_2$ crystal undergoes a phase transition from the $MgZn_2$ to the $MgCu_2$ structure. This transformation is related to the gain of symmetry of the system and appears to follow a general trend observed in intermetallic Laves compounds. By looking into the literature, one realizes that for most of the Laves (C14, C15, and C36) compounds the value of the size ratio d_{A-A}/d_{X-X} (where A represents the atom with the largest radius, X the atom with the smallest radius, and d is the minimum distance between the pair of subscripted atoms) is close to 1.2. If this size ratio is smaller than $\sqrt{3/2}$, the system generally stabilizes in the $MgZn_2$ structure; otherwise, the system stabilizes in the $MgCu_2$ structure. In fact, this same effect happens in $Ne(He)_2$, where the value of the size ratio $d_{\text{Ne-Ne}}/d_{\text{He-He}}$ becomes $\sqrt{3/2}$ at some point within the pressure interval $60 \leq P \leq 140$ GPa, which roughly coincides with P_t.

Figure 5 shows the dependence on temperature of the transition pressure P_t corresponding to the $MgZn_2 \rightarrow MgCu_2$ phase transformation in $Ne(He)_2$. [Since there is not available information about the melting behavior of the $Ne(He)_2$ crystal, we restrict here our analysis to the temperature interval $0 \leq T \leq 2000$ K basing on previous investigations performed in pure helium.[46]] Essentially, what is observed is that the value of P_t increases as the temperature is

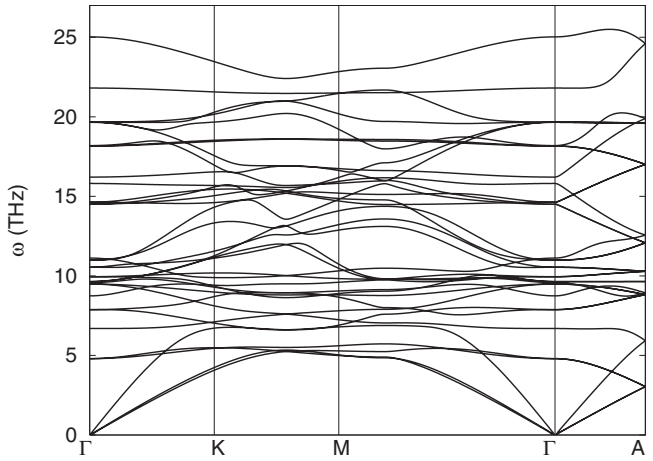

FIG. 6. Calculated phonon frequencies of $Ne(He)_2$ in the $MgZn_2$ phase structure at volume $V=6.19$ Å^3/atom ($P=33.88$ GPa).

raised. This output comes to show that ionic vibrational and entropic contributions to the total free energy (that is, F_{harm}) tend to favor the $MgZn_2$ structure over the $MgCu_2$ one. For instance, at $T=1300$ K and $V=3.61$ Å^3 ($P\sim 220$ GPa) we find that the ionic vibrational free-energy difference $\Delta F_{\text{harm}} = F_{\text{harm}}(MgZn_2) - F_{\text{harm}}(MgCu_2)$ amounts to -1 meV/atom. This result is possibly related to the fact that the $MgZn_2$ structure is less symmetric than the $MgCu_2$ structure. Nevertheless, we find that value of ΔF_{harm} in all the studied $V-T$ states is very small so that the $MgZn_2 \rightarrow MgCu_2$ transformation at $T\neq 0$ is mostly dictated by the E_{perf} contribution to the total free energy and hence close packing and symmetry arguments must also apply to this case.

In Figs. 6 and 7, we report the vibrational phonon spectra of $Ne(He)_2$ calculated for different crystal structures ($MgZn_2$ and $MgCu_2$) and pressures. In the case of the $MgZn_2$ structure, we find imaginary phonon frequencies at pressures below 12 GPa. This result can be interpreted in two different possible ways; one, that the $Ne(He)_2$ system is mechanically unstable at pressures $P\leq 12$ GPa, or the other, that DFT is not yielding the correct atomic forces because of a poor description of the dispersive interactions in the crystal. Given the lack of experiments in the low-pressure regime, it remains ambiguous which is the correct answer and, as we noted at the start of Sec. III, we leave this problem for future work.

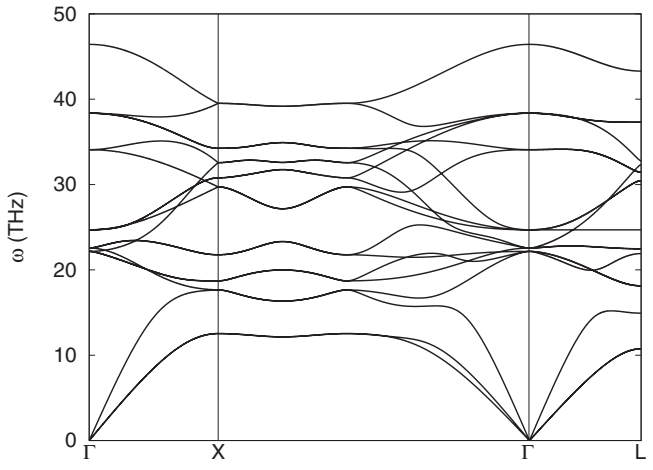

FIG. 7. Calculated phonon frequencies of $Ne(He)_2$ in the $MgCu_2$ phase structure at volume $V=3.50$ Å^3/atom ($P=215.15$ GPa).

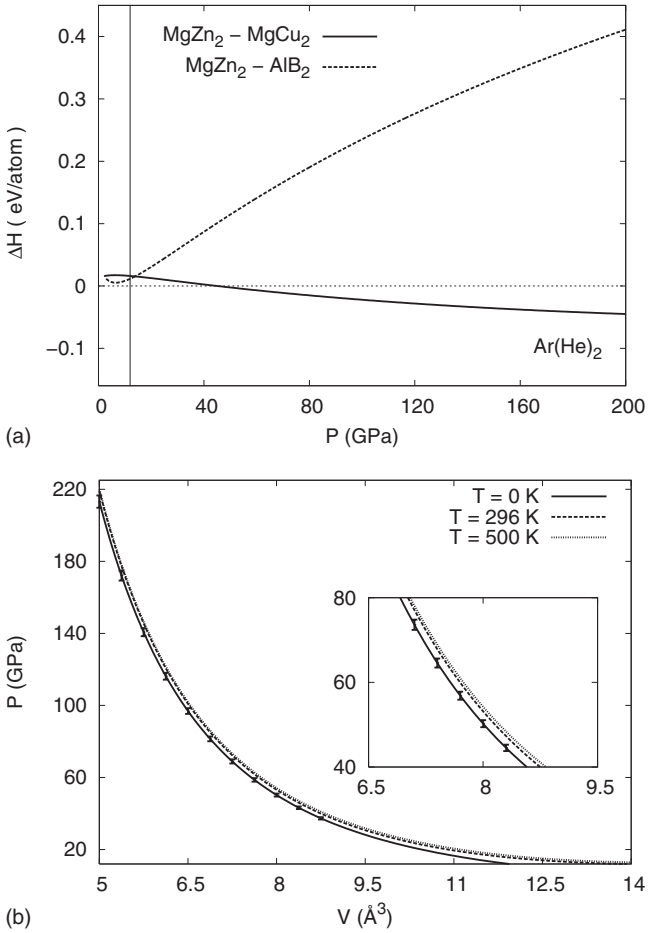

FIG. 8. Top: enthalpy difference between the $MgZn_2$-, $MgCu_2$-, and AlB_2-type phase structures of $Ar(He)_2$ under pressure and at zero temperature. The vertical solid line at 12 GPa separates the low pressure from the intermediate- and high-pressure regimes. Uncertainties associated to ΔH amount to 0.1 meV/atom. Bottom: equation of state of $Ar(He)_2$ in the AlB_2-type phase structure calculated at different temperatures. Uncertainties associated to the zero-temperature case are represented with solid vertical lines.

B. $Ar(He)_2$

Zero-temperature enthalpy differences of the $Ar(He)_2$ crystal in the $MgZn_2$, $MgCu_2$, and AlB_2 structures are shown in Fig. 8 (top) as a function of pressure. The $MgNi_2$ structure has been considered but found to be energetically not competitive so for the sake of clarity we ignore it throughout the following analysis. According to our calculations, solid $Ar(He)_2$ stabilizes in the $MgCu_2$ structure at low pressures while at pressures above $P_t=13.8(4)$ GPa it does in the AlB_2-type structure. (The enthalpy energy of the $MgZn_2$ structure is always larger than that of the $MgCu_2$ and AlB_2-type structures.) The $MgCu_2 \rightarrow AlB_2$ solid-solid transi-

TABLE II. Pressure evolution of the c/a ratio of $Ar(He)_2$ in the AlB_2-type crystal phase.

P (GPa)	202.91	101.65	52.32	27.29	14.21	7.23
c/a	1.00828	0.99067	0.95920	0.92891	0.86681	0.84107

tion that we predict, can be also understood in terms of space filling and symmetry arguments. In Table II, we show the value of the c/a ratio in the AlB_2 structure as a function of pressure; the value of such ratio is always large (that is, $0.80<c/a$) and it saturates to around 1 at high pressures. This behavior implies an overall gain of symmetry of the crystal which is manifested in the appearance of simple hexagonal sublattice of Ar atoms and progressive correspondence of first and second Ar-Ar nearest-neighbor distances. It is quite important to note that, analogously to what we find in the $Ne(He)_2$ crystal, the differential compressibility of the constituent element bond distances in $Ar(He)_2$ are very similar to those found in pure solid He and Ar.

The structural transformation that we predict appears to complete the series of solid-solid phase transitions observed in the Laves-type intermetallic compounds under compression, which is $MgZn_2 \rightarrow MgCu_2 \rightarrow AlB_2$. A similar trend is also observed in the family of Al-rare-earth binary mixtures, for instance in the $ThAl_2$ crystal. This crystal stabilizes in the AlB_2-type structure and it transitates to the $MgCu_2$ structure by effect of pressure.[47,48] In this case, the solid-solid phase transition occurs in reverse order than in $RG(He)_2$ solids because the Al-Al bonds turn out to be less compressible than the Th-Th ones [in $RG(He)_2$ systems, RG-RG bonds are less compressible than He-He bonds]. A similar behavior has been also found in YCu_2.[49]

As noted in Sec. II, it is empirically observed that the AlB_2-type structure becomes energetically competitive with respect to the family of Laves structures when roughly the value of the bond-distance ratio d_{A-A}/d_{X-X} is between 1.4 and 1.6; in fact, we find that $d_{\text{Ar-Ar}}/d_{\text{He-He}}$ amounts to 1.50 at a pressure of 14 GPa. Nevertheless, it is worthwhile noticing that the value of such ratio increases very rapidly with increasing pressure; for instance, $d_{\text{Ar-Ar}}/d_{\text{He-He}}$ is already 1.70 at a pressure of $P\sim100$ GPa. This result points toward possible pressure-induced stabilization of RG-He mixtures and, in particular, of $Ar(He)_2$, over crystal structures different from the ones considered in this work. We will comment again on such possibility in Sec. IV C.

In Fig. 8 (bottom), we report the equation of state of solid $Ar(He)_2$ calculated at different temperatures. A fit of the polynomial type in Eq. (2) to our zero-temperature results yields the value of the parameters $E_0=-0.0078(0.0009)$ eV, $V_0=22.82(0.20)$ Å^3, $K_0=0.0277(0.0007)$ eV/Å^3 [=4.44(0.11), in GPa], and $\chi=-0.265(0.020)$, where figures within parentheses indicate the associated error. As can be seen, the overall effect of taking into account vibrational ionic excitations is that of raising the zero-temperature $P-V$ curve in just few GPa, specifically $\Delta P\sim5$ GPa.

The vibrational phonon spectra of $Ar(He)_2$ at a volume of $V=9.53$ Å^3/atom ($P\sim28$ GPa) is shown in Fig. 9. There, a band gap of frequencies $\Delta\omega$ over the range of $8.0<\omega<11.5$ THz is observed. Such frequency band gap is a typical feature observed in laminarlike compounds, such as the AlB_2-type structure and comes to show the difference between "in"- and "out"-of-plane ionic vibrational modes. In general, in-plane vibrational frequencies are more energetic than the out-of-plane ones. In $Ar(He)_2$, we find only one active Raman phonon which corresponds to in-plane counterphase vibrations of the He atoms. In this case, atomic bonds and restoring forces are both quite strong. The rest of Γ-phonon modes correspond to out-of-plane vibrations of the He atoms (silent mode) or displacement of atomic Ar planes with respect to He planes (IR modes). In all these cases, restoring atomic forces are weak. A schematic representation of these phonons is enclosed in Fig. 10. We find that the width of the frequency gap seen in $Ar(He)_2$ increases with increasing pressure. For instance, $\Delta\omega$ is already about 7 THz at a volume of $V=6.37$ Å^3/atom ($P\sim100$ GPa).

C. Proposed high-P phase diagram of RG-He compounds

As noted in Secs. IV A and IV B, we find that $A-A$ and $X-X$ bond distances in $Ne(He)_2$ and $Ar(He)_2$ present practically identical dependence on pressure than found in pure Ne, Ar, and He crystals, respectively (see Fig. 4). This finding comes to show that sublattices of atoms A apparently *do not interact* with sublattices of atoms X, or in other words, that atomic short-range interactions in RG-He systems are by large the most relevant ones. Certainly, this result is in accordance with previous low-P experimental and theoretical studies which show that systems of RG species behave as ensembles of noninteracting hard spheres.[50,51] Based on this result and empirical observations, we have constructed a semiquantitative phase diagram for $RG(He)_2$ binary mixtures under pressure up to 200 GPa (see Fig. 11). Our strategy in doing this has consisted in calculating bond-distance ratios $d_{\text{RG-RG}}/d_{\text{He-He}}$ as a function of pressure (using the EOS of

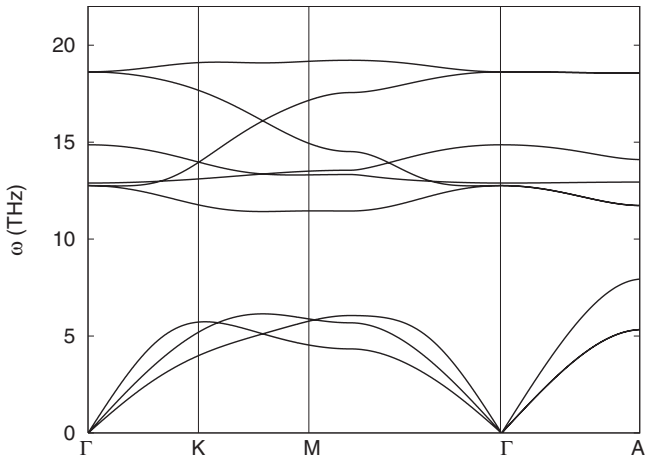

FIG. 9. Calculated phonon frequencies of $Ar(He)_2$ in the AlB_2-type phase structure at volume $V=9.53$ Å^3/atom ($P=27.88$ GPa).

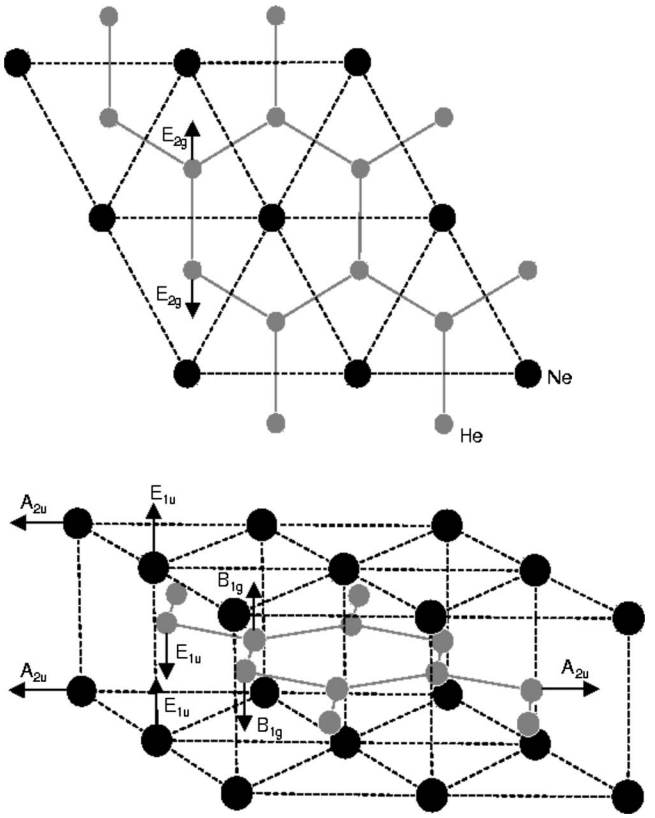

FIG. 10. Schematic representation of phonon excitations of $RG(He)_2$ in the AlB_2-type phase structure: E_{2g} (top, Raman mode), B_{1g} (bottom, silent mode), A_{2u} (bottom, infrared mode), and E_{1u} (bottom, infrared mode). Small gray spheres represent ^{4}He atoms and large black spheres RG atoms.

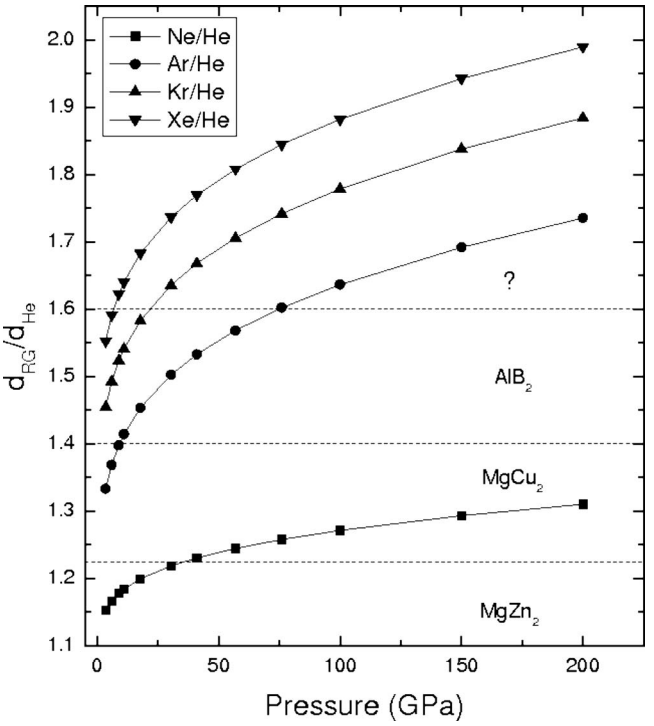

FIG. 11. Zero-temperature qualitative high-P phase diagram of binary RG-He alloys under pressure based on structural data and bond-distance ratio arguments.

pure He, Ne, Ar, Kr, and Xe found in Refs. 1, 2, 52, and 53, respectively) and then setting $\sqrt{3/2}$ and 1.40 as the value of the transition ratio for the $MgZn_2 \rightarrow MgCu_2$ and $MgCu_2 \rightarrow AlB_2$ transformations, respectively.[6,54–56] As one can see, the agreement between such semiquantitative phase diagram and our very accurate first-principles calculations for $Ne(He)_2$ and $Ar(He)_2$ is surprisingly good (especially considering that, as we have tested, the approximation used for the exchange-correlation energy may have the effect of varying the estimated transition pressures in few tens of GPa).

We have performed additional first-principles calculations in solid $Kr(He)_2$ to fully assess the reliability of our proposed generalized high-P phase diagram. We find that, equivalently to what is shown in Fig. 11, the $Kr(He)_2$ crystal is more stable in the AlB_2-type structure than in any Laves structure (by more than 60 meV/atom at low pressures), and that enthalpy energy differences among them increase with increasing pressure (so that pressure-induced phase transitions of the type $AlB_2 \rightarrow$ Laves structure are ruled out).

In conclusion, it can be said that structural predictions on RG-He systems at high-P based on very simple calculations and space-filling arguments may turn to be reasonably accurate. Nevertheless, the question about which crystal structure should become energetically more favorable than the AlB_2-type structure at extreme compression, remains unanswered and we do not find an evident candidate for it (we note this in Fig. 11 by interrogation sign). In fact, a clear trend found in RG-He systems under pressure is that of increase in symmetry so therefore, and also because of the trigonal character of the AlB_2-type structure, it could be speculated a phase transformation toward some crystal structure with primitive cubiclike symmetry.

D. Electronic structure

We have studied the dependence on pressure of the electronic structure of $Ne(He)_2$ in the $MgCu_2$ phase, $Ar(He)_2$ in the AlB_2-type phase, and $Kr(He)_2$ in the AlB_2-type phase, by performing very accurate DFT calculations (with increased k-point meshes) of the corresponding total and partial density of electronic states (DOS and pDOS, respectively). Before commenting on the results, it must be said that standard DFT has been proved to underestimate systematically the energy-band gap ΔE_g of semiconductors and insulators.[9] The essential reason for this is that DFT is an *exact* theory for the description and prediction of ground-state properties but not for excited states. Nevertheless, there is abundant evidence showing that in fact DFT yields the correct pressure-induced behavior of ΔE_g in most of crystals (that is, opening or closure).[57–60] Since our main objective here is to predict and understand the evolution of ΔE_g in $RG(He)_2$ under pressure, rather than to provide an accurate and quantitative description of the same, we suffice with standard DFT calculations and do not resort to more accurate but also computationally more demanding ansatzs like Quantum Monte Carlo and/or DFT-GW methods.

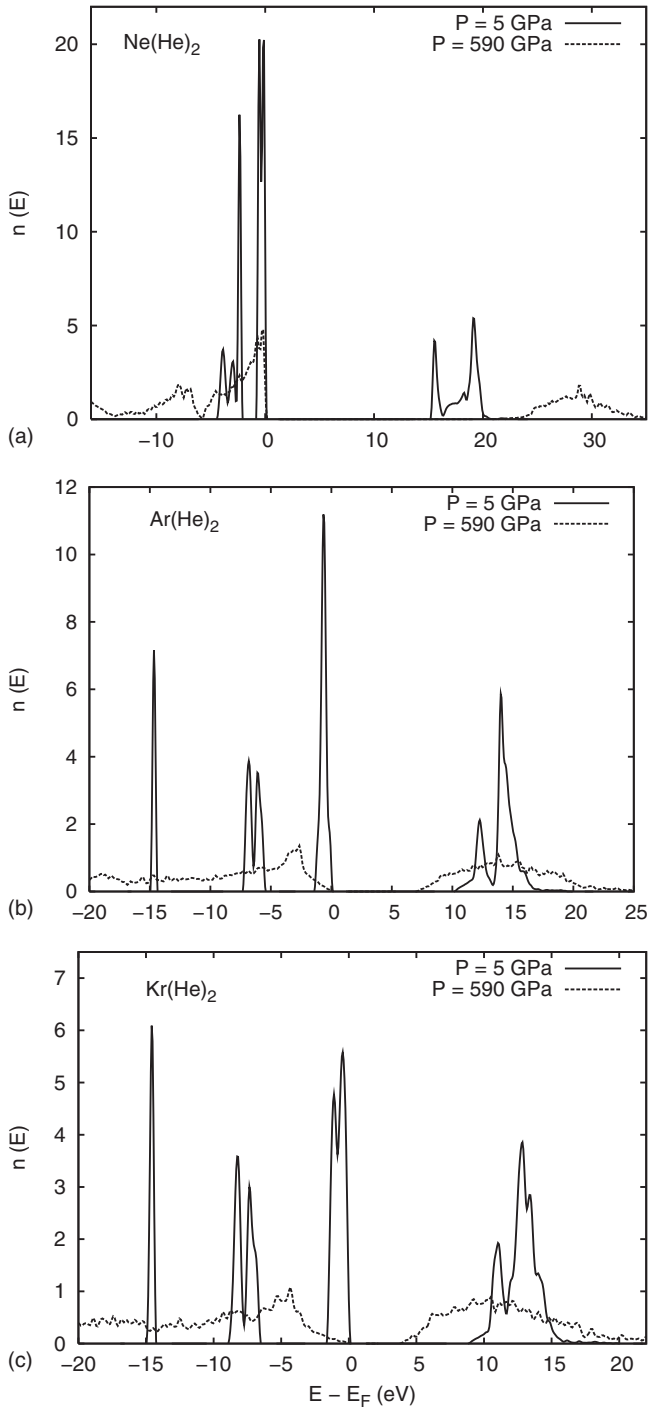

FIG. 12. Total density of electronic states of $Ne(He)_2$ in the $MgCu_2$ phase (top), $Ar(He)_2$ in the AlB_2-type phase (center), and $Kr(He)_2$ in the AlB_2-type phase (bottom) at low and high pressures.

In Fig. 12, we present results for the total DOS of $RG(He)_2$ crystals in their corresponding high-pressure phases at pressure 5 (low) and 590 (high) GPa (all Fermi-energy levels E_F have been shifted to zero). Equivalent calculations have been performed at intermediate pressures but these are not shown here for the sake of clarity. Despite the fact that at pressure $P=5$ GPa we cannot ensure the existence of the crystal phases enclosed in Fig. 12, for the reasons we commented in Sec. III, we include the corresponding electronic density of states with the sole interest of analyzing the effect of pressure on ΔE_g at fixed atomic symmetry. As can be seen, ΔE_g tends to open in $Ne(He)_2$ and to close in $Ar(He)_2$ and $Kr(He)_2$ as effect of compression. Also it is observed that the variation in the energy-band gap with pressure, $\partial \Delta E_g / \partial P$, is more negative in $Kr(He)_2$ than in $Ar(He)_2$. *A priori*, one could attempt to explain this behavior in terms of stable crystal structures and/or electronic structure of the constituent RG atoms. In order to assess the effect of the crystal structure on the pressure evolution of the energy-band gap, we have repeated identical DOS calculations in $Ar(He)_2$ but in the $MgCu_2$ structure and at different volumes. In this case, we find that at each studied pressure the value of $\partial \Delta E_g / \partial P$ is also negative but smaller than in the AlB_2-type structure. Therefore, it can be argued that the effect of the atomic structure on the pressure variation in ΔE_g is not to change its sign (that is, to reverse the closure or opening of the energy-band gap) but to vary somewhat its absolute value.

TABLE III. Relative electronic-band populations in $Ne(He)_2$ ($MgCu_2$ structure) and $Kr(He)_2$ (AlB_2-type structure) calculated over the energy interval $E_F \leq E \leq E_F+20$ eV, E_F being the Fermi-energy level (figures within parentheses correspond to integrated partial DOSs over the energy interval E_F-20 eV $\leq E \leq E_F$). P_l is equal to 5 GPa while P_h is 590 GPa.

Type (%)	$Ne(He)_2$		$Kr(He)_2$	
	P_l	P_h	P_l	P_h
s	47.3(38.2)	7.5(36.4)	24.7(41.6)	5.9(37.5)
p	44.0(61.7)	48.0(62.3)	18.2(55.9)	10.9(52.8)
d	8.7(0.1)	44.5(1.3)	57.1(2.5)	83.2(9.7)

Furthermore, we have computed the partial DOSs (*s*, *p*, and *d* types) of $Ne(He)_2$ in the $MgCu_2$ structure and $Kr(He)_2$ in the AlB_2-type structure at low and high pressures in order to fully understand the pressure evolution of the corresponding energy-band gaps. In Table III, we report the value of the relative *s*, *p*, and *d* electronic-band populations over energy intervals spanning 20 eV below and above the Fermi level. We obtain these values by proper integration of the corresponding partial and total DOSs. There, it is observed that electronic orbitals below the Fermi level are mostly of the *s* and *p* types in both $Ne(He)_2$ and $Kr(He)_2$ crystals at low and high pressures; on the other side, electronic *d* orbitals are only abundant in $Kr(He)_2$ and in the energy region $E_F<E$ (conduction band). Another interesting result is that the population of *d* orbitals in the conduction band raises significantly in all the cases by effect of increasing pressure.

Conclusions derived from Table III point toward plausible argument explaining the behavior of ΔE_g in $RG(He)_2$ solids, namely, under pressure, the energy-band gap will close (open) whether the population of *d* orbitals in the conduction band (mostly provided by RG atoms) is large (sparse). This is in accordance with the well-known effect that electronic *d*-orbitals experiment smaller increase in energy under pressure than *s* and *p* states do since the first are more localized in space;[33,61] therefore, given that electronic *s* and *p* states

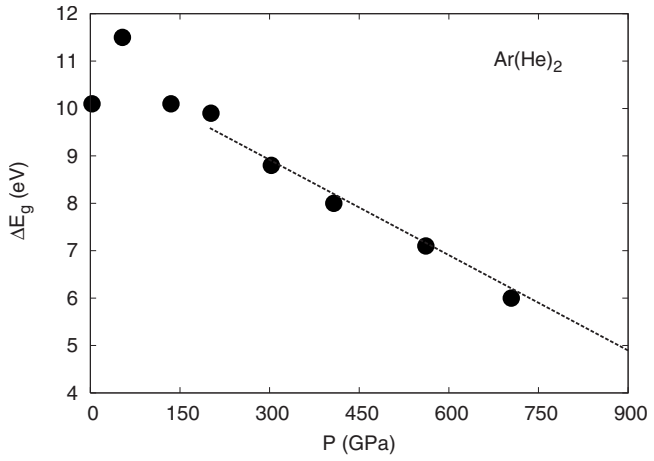

FIG. 13. Evolution of the electronic-band gap of $Ar(He)_2$ in the AlB_2-type phase structure with pressure. The metallization pressure of helium in such compound is estimated to be of order $P_{metal} \sim 1630$ GPa.

are always large in number in the valence band ($E \leq E_F$), the sign of $\partial \Delta E_g / \partial P$ will depend basically on the population of electronic d states above the Fermi level.

In Fig. 13, we show the pressure evolution of ΔE_g in $Ar(He)_2$ (AlB_2-type structure) up to a pressure of 750 GPa. As can be seen there, ΔE_g opens slightly at pressures within the range $0 \leq P \leq 75$ GPa while it clearly tends to close at higher pressures. This effect can be explained in similar terms than the ones mentioned in the previous paragraph: a certain pressure is necessary to initially enhance the population of electronic d states in the conduction band (Ar atoms provide less concentration of d states than Kr atoms at normal conditions), so the energy-band gap opens; this regime is transitory and eventually, when pressure is sufficiently high, ΔE_g starts to close.

In the same figure, it is shown that the value of $\partial \Delta E_g / \partial P$ is practically a constant at high pressures. By performing a simple linear extrapolation, we roughly estimate the metallization pressure P_{metal} of the crystal [that is, $\Delta E_g(P_{metal})=0$] to be ~ 1630 GPa. It is interesting to note that, in spite of the deficiencies of customary DFT at estimating the correct value of ΔE_g, our prediction for the nonmetallic to metallic pressure-induced transition in $Ar(He)_2$ is about one order of magnitude smaller than the one obtained in pure helium with similar computational approaches than used here, $P_{metal}^{GGA}=15\,420$ GPa,[62] or with the more complex but also very accurate diffusion Monte Carlo method, $P_{metal}^{DMC}=25\,700$ GPa.[9] This finding is at odds to what is predicted by Matsumoto and Nagara[14] in the $Ar(H_2)_2$ crystal.

V. DISCUSSION AND CONCLUSIONS

There are several analogies between the hydrogen molecule and the helium atom. Both are bosonic entities, light weighted and possess the same number of electrons. Also, bulk solid H_2 and ^{4}He are both stable in the hexagonal closed-packed structure and present very similar electronic density profile when looking at a same interparticle

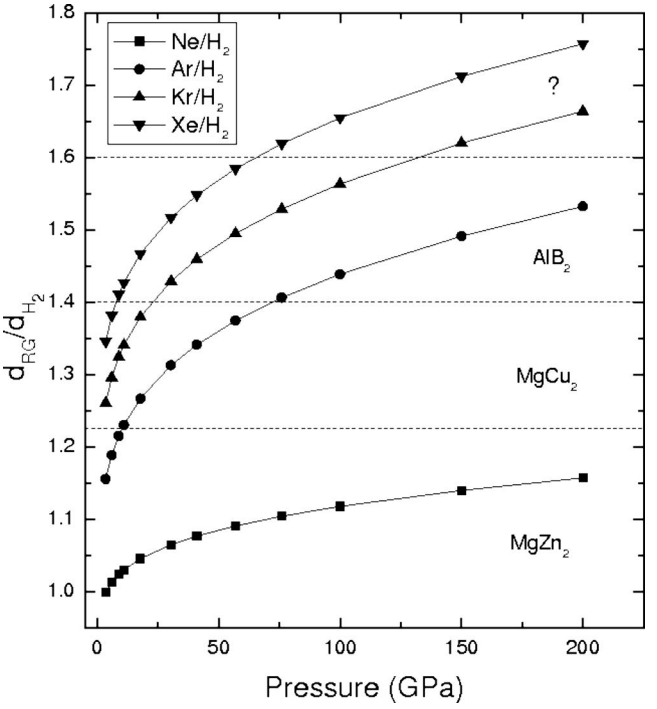

FIG. 14. Zero-temperature qualitative high-P phase diagram of binary RG-H_2 alloys under pressure based on existing experimental data and atomic size-ratio arguments.

separation.[63] Furthermore, compounds such as $Ar(H_2)_2$ have been realized experimentally and found to stabilize in the Laves and AlB_2-type structures.[10,11,14] Because all these similarities and the good qualitative agreement between accurate first-principles calculations and atomic size-ratio arguments in $RG(He)_2$ systems, it seems natural to sketch a semiquantitative generalized phase diagram, equivalent to that shown in Sec. IV C, also for $RG(H_2)_2$ crystals. In Fig. 14, we present such phase diagram where we have considered all possible RG-H_2 mixtures (made the exception of He) up to a pressure of 200 GPa and based on the data found in Ref. 63 for H_2.

For a given pressure, H_2-H_2 bond distances in pure hydrogen are larger than He-He atomic distances in bulk helium, so curves in Fig. 14 appear shifted downward with respect to the ones reported in Fig. 11. A quite interesting result coming out from our semiquantitative phase diagram is the pressure-induced behavior of the $Ar(H_2)_2$ crystal. This appears to stabilize first in the $MgZn_2$ Laves structure, then in the $MgCu_2$ Laves structure, and finally in the AlB_2-type structure. This result differs from the generally accepted series of pressure-induced transformations taking place in $Ar(H_2)_2$, which is $MgZn_2 \rightarrow AlB_2$. To the best of our knowledge the $MgCu_2$ Laves structure has not been considered in any previous investigation of RG-H_2 mixtures. We recall here that solid $Ar(H_2)_2$ has raised much attention in the last few years because possible induced molecular dissociation and subsequent metallization of hydrogen at much lower pressures than predicted in bulk H_2.[10,11] The fundamental reason for this proposition is that, at a fixed pressure, intermolecular H_2-H_2 distances are shorter in such compound than in pure hydrogen. In view of this argument and Fig. 14, it can be

suggested that solid $Kr(H_2)_2$ might turn out to be even a better candidate than $Ar(H_2)_2$ where to observe the so long-awaited pressure-induced metallization of hydrogen since the first already stabilizes in the AlB_2-type structure at low pressures.

Certainly, the generalized high-P phase diagram of Fig. 14 must not be interpreted literally since its character is qualitative and may contain some serious imprecisions. For instance, the $MgCu_2 \rightarrow AlB_2$ transformation in $Ar(H_2)_2$ is predicted to occur at a pressure of ~ 75 GPa, which is much smaller than the transition pressure reported for the $MgZn_2 \rightarrow AlB_2$ transformation in the same crystal obtained with DFT ($P_t \sim 240$ GPa).[14] Nevertheless, we believe that the $MgCu_2$ Laves structure must not be ignored in the study of RG-H_2 compounds and it is our intention to carry out further and improved calculations of this kind of systems contemplating such possibility.

In conclusion, we have performed a comprehensive first-principles study of the energetic and structural properties of solid $Ne(He)_2$ and $Ar(He)_2$ mixtures, up to a pressure of 300 GPa and over the temperature interval $0 \leq T \leq 2000$ K. As a result, we predict pressure-induced solid-solid transformations in both systems which involve the family of Laves and AlB_2-type structures. Based on empirical observations and space-filling arguments, we drawn a general phase diagram for the whole family of RG-$(He)_2$ crystals up to a pressure of 200 GPa in which we map out general structural trends; this is shown to be in excellent qualitative agreement with *ab initio* calculations. A similar construction is also done for RG-$(H_2)_2$ crystals and we find that the $MgCu_2$ Laves structure might turn out to be competitive with respect to the $MgZn_2$- and AlB_2-type structures. Additionally, we explore the pressure evolution of the energy-band gap in some $RG(He)_2$ compounds and elaborate an argument based on band-theory concepts which explains the observed trends.

ACKNOWLEDGMENTS

D.E. acknowledges financial support of the MICINN of Spain under Grant Nos. CSD2007-00045 and MAT2007-65990-C03-01 and by the Generalitat Valenciana under Grant No. GVPRE-2008-112.

[1] A. Dewaele, F. Datchi, P. Loubeyre, and M. Mezouar, Phys. Rev. B **77**, 094106 (2008).
[2] D. Errandonea, R. Boehler, S. Japel, M. Mezouar, and L. R. Benedetti, Phys. Rev. B **73**, 092106 (2006).
[3] P. Loubeyre, M. Jean-Louis, R. LeToullec, and L. Charon-Gerard, Phys. Rev. Lett. **70**, 178 (1993).
[4] C. Qi-Feng, C. Ling-Cang, J. Fu-Qian, and C. Dong-Quan, Chin. Phys. Lett. **22**, 2005 (2005).
[5] T. Ohba, Y. Kitano, and Y. Komura, Acta Crystallogr., Sect. C: Cryst. Struct. Commun. **40**, 1 (1984).
[6] R. L. Berry and G. V. Raynor, Acta Crystallogr. **6**, 178 (1953).
[7] R. D. Hoffman and R. Pottgen, Z. Kristallogr. **216**, 127 (2001).
[8] W. B. Pearson, Acta Crystallogr. **17**, 1 (1964).
[9] S. A. Khairallah and B. Militzer, Phys. Rev. Lett. **101**, 106407 (2008).
[10] P. Loubeyre, R. Letoullec, and J.-P. Pinceaux, Phys. Rev. Lett. **72**, 1360 (1994).
[11] S. Bernard, P. Loubeyre, and G. Zerah, Europhys. Lett. **37**, 477 (1997).
[12] L. Ulivi, R. Bini, P. Loubeyre, R. LeToullec, and H. J. Jodl, Phys. Rev. B **60**, 6502 (1999).
[13] R. Hemley, Annu. Rev. Phys. Chem. **51**, 763 (2000).
[14] N. Matsumoto and H. Nagara, J. Phys.: Condens. Matter **19**, 365237 (2007).
[15] C. Cazorla and J. Boronat, J. Phys.: Condens. Matter **20**, 015223 (2008).
[16] C. Cazorla and J. Boronat, Phys. Rev. B **77**, 024310 (2008).
[17] M. Dion, H. Rydberg, E. Schröder, D. C. Langreth, and B. I. Lundqvist, Phys. Rev. Lett. **92**, 246401 (2004).
[18] M. Dion, Ph.D. thesis, Rutgers University, 2004.
[19] M. A. Basanta, Y. J. Dappe, J. Ortega, and F. Flores, Europhys. Lett. **70**, 355 (2005).
[20] O. Delgado-Friedrichs, M. O'Keeffe, and O. M. Yaghi, Acta Crystallogr., Sect. A: Found. Crystallogr. **62**, 350 (2006).
[21] R. M. Martin, *Electronic Structure* (Cambridge University Press, Cambridge, 2004).
[22] J. Kohanoff, *Electronic Structure Calculations for Solids and Molecules: Theory and Computational Methods* (Cambridge University Press, Cambridge, 2006).
[23] M. J. Gillan, D. Alfè, J. Brodholt, L. Vočadlo, and G. D. Price, Rep. Prog. Phys. **69**, 2365 (2006).
[24] C. Cazorla, D. Alfè, and M. J. Gillan, Phys. Rev. B **77**, 224103 (2008).
[25] Y. Wang and J. P. Perdew, Phys. Rev. B **44**, 13298 (1991).
[26] D. M. Ceperley and B. J. Alder, Phys. Rev. Lett. **45**, 566 (1980).
[27] D. Vanderbilt, Phys. Rev. B **41**, 7892 (1990).
[28] P. E. Blöchl, Phys. Rev. B **50**, 17953 (1994).
[29] G. Kresse and D. Joubert, Phys. Rev. B **59**, 1758 (1999).
[30] O. K. Andersen, Phys. Rev. B **12**, 3060 (1975).
[31] D. Singh, *Planewaves, Pseudopotentials and the LAPW method* (Kluwer Academic, Boston, 1994).
[32] G. Kresse and J. Furthmüller, Phys. Rev. B **54**, 11169 (1996).
[33] C. Cazorla, M. J. Gillan, S. Taioli, and D. Alfè, J. Chem. Phys. **126**, 194502 (2007).
[34] N. D. Drummond and R. J. Needs, Phys. Rev. B **73**, 024107 (2006).
[35] Z. Nabi, L. Vitos, B. Johansson, and R. Ahuja, Phys. Rev. B **72**, 172102 (2005).
[36] Estimated energy per atom of $Ne(He)_2$ in the $MgZn_2$ structure at $V=4.30$ Å^3 and different k-point grids: 1.38436 eV ($14\times14\times7$) and 1.38438 eV ($18\times18\times9$); estimated energy per atom of $Ne(He)_2$ in the $MgCu_2$ structure at $V=4.30$ Å^3 and different k-point grids: 1.38487 eV ($14\times14\times14$) and 1.38480 eV ($18\times18\times18$).
[37] H. J. Monkhorst and J. D. Pack, Phys. Rev. B **13**, 5188 (1976).
[38] F. Birch, J. Geophys. Res. **83**, 1257 (1978).
[39] D. Alfè, program available at http://chianti.geol.ucl.ac.uk/~dario (1998).

[40] D. Alfè, Comm. Comp. Phys. (to be published).
[41] G. Kresse, J. Furthmüller, and J. Hafner, Europhys. Lett. **32**, 729 (1995).
[42] D. Alfè, G. D. Price, and M. J. Gillan, Phys. Rev. B **64**, 045123 (2001).
[43] R. Lacomba-Perales, D. Errandonea, D. Martinez-Garcia, P. Rodriguez-Hernandez, S. Radescu, A. Mujica, A. Munoz, J. C. Chervin, and A. Polian, Phys. Rev. B **79**, 094105 (2009).
[44] D. Errandonea, R. S. Kumar, F. J. Manjon, V. V. Ursaki, and E. V. Rusu, Phys. Rev. B **79**, 024103 (2009).
[45] J. Wittlinger, R. Fischer, S. Werner, J. Schneider, and H. Schulz, Acta Crystallogr., Sect. B: Struct. Sci. **B53**, 745 (1997).
[46] L. Koči, R. Ahuja, A. B. Belonoshko, and B. Johansson, J. Phys.: Condens. Matter **19**, 016206 (2007).
[47] K. H. J. Buschow and H. J. van Daal, Phys. Rev. Lett. **23**, 408 (1969).
[48] B. K. Godwal, V. Vijaykumar, S. K. Sikka, and R. Chidambaram, J. Phys. F: Met. Phys. **16**, 1415 (1986).
[49] A. Lindbaum, S. Heathman, G. Kresse, M. Rotter, E. Gratz, A. Schneidewind, G. Behr, K. Liftin, T. Le Bihan, and P. Svodoba, J. Phys.: Condens. Matter **12**, 3219 (2000).
[50] S. Bukshpan, P. Hendrickx, K. Milants, and H. Pattyn, Phys. Rev. B **45**, 497 (1992).
[51] J. L. Barrat, M. Baus, and J. P. Hansen, Phys. Rev. Lett. **56**, 1063 (1986).
[52] A. Dewaele, J. H. Eggert, P. Loubeyre, and R. Le Toullec, Phys. Rev. B **67**, 094112 (2003).
[53] D. Errandonea, B. Schwager, R. Boehler, and M. Ross, Phys. Rev. B **65**, 214110 (2002).
[54] J. M. Murray and J. V. Sanders, Philos. Mag. A **42**, 721 (1980).
[55] D. J. Thoma and J. H. Perepezko, J. Alloys Compd. **224**, 330 (1995).
[56] W. B. Pearson, Acta Crystallogr., Sect. B: Struct. Crystallogr. Cryst. Chem. **37**, 1183 (1981).
[57] D. Y. Kim, R. H. Scheicker, S. Lebègue, J. Prasongkit, B. Arnaud, M. A. Rouani, and R. Ahuja, Proc. Natl. Acad. Sci. U.S.A. **105**, 16454 (2008).
[58] Y. Duan and D. C. Sorescu, Phys. Rev. B **79**, 014301 (2009).
[59] G. Rollmann, A. Rohrbach, P. Entel, and J. Hafner, Phys. Rev. B **69**, 165107 (2004).
[60] R. Franco, P. Mori-Sanchez, J. M. Recio, and R. Pandey, Phys. Rev. B **68**, 195208 (2003).
[61] M. Ross, R. Boehler, and P. Söderlind, Phys. Rev. Lett. **95**, 257801 (2005).
[62] P. M. Kowalski, S. Mazevet, D. Saumon, and M. Challacombe, Phys. Rev. B **76**, 075112 (2007).
[63] I. Silvera, Rev. Mod. Phys. **52**, 393 (1980).